A Navigation Model of the Continuous Outgassing Field Around a Comet

D. J. Scheeres,[1] S. Bhargava,[2] and A. Enzian[3]

A model describing the continuous portion of a comet's outgassing pressure field is presented. Applications of the model to spacecraft navigation are discussed, noting that such models are similar to a gravity field representation and, hence, can be estimated with radio metric tracking of a spacecraft. The model is fit to numerically generated outgassing fields for the comets Tempel-1 and Wirtanen. The parameter coefficients for these fits are presented along with comparisons showing that the analytical form fits the numerically computed fields well.

I. Introduction

Missions to comets are currently of interest to NASA's Office of Space Science, as is borne out by the number of ongoing, approved, and planned missions to comets (Stardust, Contours, Deep Impact, and Comet Nucleus Sample Return missions). They are also of interest to the international space science community, as is evident from the commitment of the European Space Agency (ESA) to the Rosetta mission. Two of these missions, the proposed Comet Nucleus Sample Return mission and the approved Rosetta mission, have periods of orbital operations about a comet. In order to support spacecraft navigation for these orbital missions, it is necessary that realistic force models of the comet environment be developed. Specifically, it is important to develop appropriately parameterized force models for comets before the final design of the navigation software used to execute these missions is developed.

For both spacecraft navigational and scientific measurement purposes, it is important for an accurate model of the outgassing pressure field about a comet to be developed for use in estimation of that field. Due mainly to the lack of observations and simulations of these fields, earlier models [2,5] in general have used fairly simple models for recreating the pressure field. With recent advances in comet measurement capability and numerical comet pressure field simulation, it now makes sense to consider more detailed models of a comet pressure field. This article presents a very general parameterization of a comet pressure field and shows that it can be used to accurately fit detailed numerical models of comet outgassing. A brief discussion of the estimation of the pressure field using this model also is given. The model is a generalization of the standard gravity field model used successfully in spacecraft navigation. We consider only the continuous portion of the outgassing field; jets are not considered in the current analysis.

---

[1] Department of Aerospace Engineering, The University of Michigan, Ann Arbor.

[2] Graduate Student, Department of Aerospace Engineering and Engineering Mechanics, Iowa State University, Ames.

[3] Post-doctoral fellow, Galileo NIMS Team.

The research described in this publication was carried out by the Jet Propulsion Laboratory, California Institute of Technology, under a contract with the National Aeronautics and Space Administration.

In this article, we develop a parameterized form for the evaluation of a comet pressure field and fit it to a numerically computed comet outgassing field [1]. Our initial aim is to show that the proposed model, based on current theories about comet outgassing, can capture the basic structure of an outgassing field. To this end, we define the parameterized field, fit it to a series of comet outgassing models for the comets Tempel-1 and Wirtanen, and evaluate the goodness of the fit. We find that our simplified force model does an adequate job of capturing the complex form of the outgassing field. Our formulation implicitly assumes that the relative speed between the spacecraft and outgassing molecules is large. As the assumed outgassing speed is on the order of 100 m/s, this allows our formulation to be applied to the orbital motion of a spacecraft about a comet, where the spacecraft speed is much less than the outgassing molecules, or to the flyby trajectory of a spacecraft by a comet, where the spacecraft speed is much larger than the outgassing molecules. Future investigations into the characterization of comet outgassing for navigation models will investigate the effect of comet shape and rotation, modeling of outgassing jets, and modeling of outgassing strength with changing heliocentric distances.

II. Analytic Representation of a Comet Pressure Field

A. Motivations for Analytic Representations of Comet Pressure Fields

To derive predictions of a comet's pressure field involves the sophisticated modeling of molecular and gas dynamics, a process which is time consuming and a strong function of boundary conditions, initial estimates, and appropriate approximations [1]. This approach is not well suited to the production of "generic" models of a comet pressure field for use in spacecraft trajectory navigation and design for a comet orbiter. These numerical approaches also do not provide a direct means with which to conveniently fit spacecraft tracking and navigation data to specific theories of comet coma dynamics. These problems can be alleviated if a general class of analytical representations is developed that can parameterize a comet's pressure field—which is the crucial mechanical quantity that will have an observable effect on a spacecraft's trajectory. From the viewpoint of scientific measurements, the development of pressure field parameterizations will be useful in the reduction of spacecraft tracking data as it will enable the estimation of comet pressure field strength as a function of position about the comet.

There are perhaps more dissimilarities between a comet pressure field and its gravity field, but enough similarities exist to posit a similar estimation scheme for the two. While a comet nucleus' gravity field is tied directly to the body in question, a comet pressure field instead will involve a body-fixed term modulated by the amount of solar energy impinging on the body (i.e., a function of its phase angle), and thus will have a markedly different signature from a gravity field. Also, while a gravity field's higher moments decay swiftly with increasing radius, a comet pressure field will retain its characteristic angular distribution over a range of radii, with the strength of the pressure decreasing uniformly as $1/r^2$.

While these differences in distribution may allow for the effects of gravity and pressure to be decoupled, to some extent, in the estimation process, the most prudent comet pressure field estimation scheme first would estimate the comet nucleus gravity field during a period of low cometary activity and then estimate the comet pressure field at different times and at different levels of activity. Due to the dynamic nature of comet activity, the "field" as defined by the analytic representation will be changing as a function of time, with stochastic fluctuations as well as changes in its mean properties. It is possible to account for these variations with current spacecraft estimation techniques, treating the parameters describing the comet pressure field as stochastic parameters with assigned steady-state uncertainties and correlation times [2]. While the level of precision will never reach that possible with gravity field estimation, this basic approach to measurement should provide valuable information about the basic strength and structure of the pressure field about a comet.

B. Spherical Harmonic Representation of a Pressure Field

We use a spherical harmonic expansion to capture the distribution of the pressure field as a function of position about the comet. The current situation is simplified as the surface of the comet is assumed to be a simple sphere; thus, we do not see temporal variations in the pressure field as the comet rotates. Analysis of the velocity vector field of the numerically computed pressure fields indicates that the pressure acts primarily in the radial direction, and thus we assume that the pressure field acts purely in the radial direction. These approximations can be investigated and relaxed in future studies.

The natural coordinate frame to use in describing the comet pressure field defines the location of a test point by its radial distance from the comet center, r; its cone angle, ϕ, as measured from the comet–Sun line to the test point; and its clock angle, λ, as measured in the terminator plane of the comet (the plane normal to the comet–Sun line). The configuration of the coordinate frame used is shown in Fig. 1.

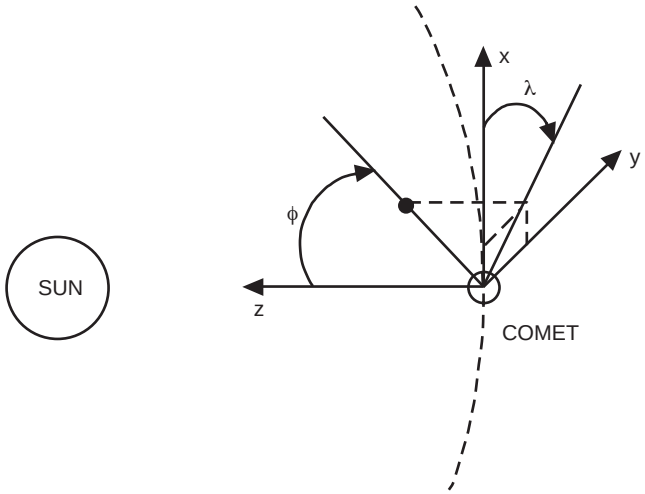

Fig. 1. Comet coordinate frame.

The z-axis points directly towards the Sun; the x-axis points in the direction of comet motion in its orbital plane; and the y-axis is chosen to complete the right-hand coordinate frame. Thus, any direction around the comet can be represented by the unit vector, $\hat{u}$, as

$$\hat{u} = \sin(\phi)\cos(\lambda)\hat{X} + \sin(\phi)\sin(\lambda)\hat{Y} + \cos(\phi)\hat{Z}$$

The drag pressure at any point near the comet is assumed to be a function of the radial distance from the comet, r; the subsolar latitude, ϕ; and the subsolar longitude, λ.

As the radius of the test point varies, we expect to see a $1/r^2$ variation in the pressure strength, while, as the cone angle varies from 0 (Sun side) to π (dark side), we expect to see the strength of the pressure drop from its maximum value to near zero. To capture such variations, we use a modified form of the spherical harmonic expansion:

$$\mathcal{P}_a(r,\phi,\lambda) = \frac{\mathcal{P}_d}{r^2}\left[1 + \sum_{i=1}^{N}\sum_{j=0}^{i} P_{ij}(\cos\phi)\left\{\alpha_{ij}\cos(j\lambda) + \beta_{ij}\sin(j\lambda)\right\}\right] \tag{1}$$

where the P_{ij} are associated Legendre functions, and the parameters $\mathcal{P}_d$, α_{ij}, and β_{ij} are chosen to fit the comet pressure field. The expansion is orthogonal, allowing the coefficients to be measured and fit independently of each other. The value of the pressure field is generally expressed in pascals (N/m^2), meaning that the parameter $\mathcal{P}_d$ has units of Pa-km^2, if r is measured in km, while the coefficients α_{ij} and β_{ij} are dimensionless.

C. Force Computations Using the Analytical Pressure Field

For the current application to outgassing pressure acting on a spacecraft in orbit about a comet, we assume that the speed of the gas is large with respect to the speed of the spacecraft, and, hence, the pressure field acts in the direction of the gas flow. Then, for a spacecraft with mass M, projected surface area A, position vector $\mathbf{r}$, and angular coordinates ϕ and λ, the force acting on it is

$$\mathbf{F} = \frac{\mathcal{P}_a(r, \phi, \lambda)A}{M}\hat{\mathbf{v}}_g \tag{2}$$

where $\hat{\mathbf{v}}_g$ is the direction of the gas velocity, assumed to be radial outward from the comet center. As the spacecraft orientation is varied, the net direction of the pressure force also will change. Due to this coupling, it is important that the attitude of the spacecraft be known whenever the pressure field is being estimated or used to predict the nongravitational forces acting on the spacecraft.

We can generalize our formulation to the more general case when the spacecraft may have a large speed relative to the gas speed, such as would be encountered during a hyperbolic flyby of a comet. In this case, we want the density of the gas as a function of position. Since the speed of the gas molecules is approximately constant [1], we can define the density:

$$\tilde{\mathcal{P}}_a = \frac{\mathcal{P}_a}{v_g^2} \tag{3}$$

where v_g is the gas speed. Then the force that the spacecraft experiences will be proportional to the relative speed between the gas and the spacecraft squared. For this more general case, we can re-express the force acting on the spacecraft as

$$\mathbf{F} = \frac{\tilde{\mathcal{P}}_a(r, \phi, \lambda)A}{M}\left[(\mathbf{v}_g - \mathbf{V}) \times (\mathbf{v}_g - \mathbf{V})\right]\frac{(\mathbf{v}_g - \mathbf{V})}{|\mathbf{v}_g - \mathbf{V}|} \tag{4}$$

where $\mathbf{v}_g$ is the velocity vector of the gas molecules, nominally along the radial direction (and usually on the order of 1 km/s), and $\mathbf{V}$ is the velocity vector of the spacecraft relative to the comet center. For a low-speed, orbiting spacecraft, we recover our standard form, while for a high-speed, hyperbolic flyby, we find that the gas pressure acts as a drag on the spacecraft.

A few notes are in order as to the strength of the comet pressure field. For any given comet, the predicted pressure strength may be uncertain to orders of magnitude, depending on what assumptions are made. To make this discussion more pointed, we will use the predicted pressure field from the periodic comet Tempel-1 at a distance of 2 AU from the Sun [1]. The maximum value of pressure found for this computation (at the subsolar point) is of the order 0.001 Pa at 19.5 km from the comet center (see Fig. 2 later). Assuming a spacecraft-mass-to-area ratio of 30 kg/m^2 leads to a total pressure field acceleration acting on the spacecraft at the subsolar point of

$$a_o \sim \frac{1.27 \times 10^{-5} \mathrm{km}^3/\mathrm{s}^2}{r^2} \tag{5}$$

where the radius, r, is measured in km. This level of acceleration is equivalent to the gravitational attraction of a sphere with density 1 g/cm^3 and a radius of 3.5 km. Note that the spacecraft will feel this maximum pressure only if flying over the subsolar point and most of the time will experience a much smaller pressure force. Despite this, we see that the effect of comet pressure can significantly perturb the motion of a spacecraft [4].

D. Review of Spherical Harmonics and Legendre Polynomials

Spherical harmonics occur in a variety of physical problems that are solved by separation of variables in spherical coordinates. The Legendre polynomials, defined as $P_i(\cos\phi)$, satisfy an important orthogonality relation,

$$\int_0^\pi P_i(\cos\phi) P_j(\cos\phi) \sin(\phi) d\phi = 0 \tag{6}$$

for $i \neq j$, and

$$\int_0^\pi P_i^2(\cos\phi) \sin(\phi) d\phi = \frac{2}{2i+1} \tag{7}$$

This property also is shared by the associated Legendre polynomials, where

$$\int_0^\pi P_{ij}(\cos\phi) P_{kl}(\cos\phi) \sin(\phi) d\phi = 0 \tag{8}$$

for $i \neq k, j \neq l$, and

$$\int_0^\pi P_{lm}^2(\cos\phi) \sin(\phi) d\phi = \frac{(l+m)!}{(l-m)!} \frac{2}{2l+1} \tag{9}$$

The associated Legendre functions P_{lm} for $l = 0, 1, 2, 3$ are listed in Table 1. Further explanation on the theory of Legendre polynomials can be found in [3].

Table 1. Associated Legendre functions.

l	m	$P_{lm}(\cos\phi)$
0	0	1
1	0	$\cos\phi$
1	1	$\sin\phi$
2	0	$\frac{1}{2}(3\cos^2\phi - 1)$
2	1	$3\cos\phi\sin\phi$
2	2	$3\sin^2\phi$
3	0	$\frac{1}{2}(5\cos^3\phi - 3\cos\phi)$
3	1	$\frac{1}{2}(15\cos^2\phi - 3)\sin\phi$
3	2	$15\cos\phi\sin^2\phi$
3	3	$15\sin^3\phi$

III. Fitting the Model to a Numerically Computed Field

For the evaluation of this model, we must devise a scheme that assigns the parameters of the model to reconstruct a numerically derived comet pressure field. This problem is different from the estimation problem, which seeks to compute the parameter values given a specific set of measurements. Here we know the pressure field and wish to find the best analytical fit to this field over the interval of definition. If our analytic form can fit the numerical field to sufficient accuracy, then it will be useful for modeling and estimation applications.

To perform the fit, we use a field computed for a given comet at a given distance from the Sun, designating the numerically computed pressure field distribution as $\mathcal{P}_n(r,\phi,\lambda)$, which is stored in a numerical grid format that must be interpolated (over different species and spatial variables) in order to find the total pressure acting at a given location [1]. Given $\mathcal{P}_n$, we fit the analytic representation to it over the range of definition of the data set. To do this, we use a least-squares formulation that minimizes the functional J':

$$J' = \int_{\mathcal{V}} J(r,\phi,\lambda)dV \tag{10}$$

$$J(r,\phi,\lambda) = \left(r^2\mathcal{P}_n - r^2\mathcal{P}_a\right)^2 \tag{11}$$

where $\mathcal{V}$ is the total volume over which the numerical results are defined. The minimization process chooses the parameters $\mathcal{P}_d$, α_{ij}, and β_{ij} to minimize the functional J'. Computing the partials $\partial J'/\partial\alpha_{ij}$ and $\partial J'/\partial\beta_{ij}$ yields specific formulas for the α_{ij} and β_{ij} as a function of the integral of the numerical field over the volume to which the representation is being fit.

The specific steps used in our process are detailed below. Let $\mathcal{P}_n(r,\phi,\lambda)$ be the numerical drag pressure field obtained from the numerical simulation of the comet force environment. Let $\mathcal{P}_a(r,\phi,\lambda)$ be the analytical drag pressure field modeled as represented in Eq. (1). Setting

$$\tilde{\alpha}_{00} = \mathcal{P}_d$$

(and, therefore, $\alpha_{00} = 1.0$) and

$$\tilde{\alpha}_{ij} = \mathcal{P}_d \alpha_{ij}$$

$$\tilde{\beta}_{ij} = \mathcal{P}_d \beta_{ij}$$

we obtain

$$\mathcal{P}_a(r,\phi,\lambda) = \frac{1}{r^2}\left[\sum_{i=0}^{N}\sum_{j=0}^{i} P_{ij}(\cos\phi)\left[\tilde{\alpha}_{ij}\cos(j\lambda) + \tilde{\beta}_{ij}\sin(i\lambda)\right]\right] \tag{12}$$

Note that the $\tilde{\beta}_{n0} = 0$, identically. To create a least-squares fit of the parameters to the numerical field, let

$$J(r,\phi,\lambda) = \frac{1}{2}|r^2\mathcal{P}_n(r,\phi,\lambda) - r^2\mathcal{P}_a(r,\phi,\lambda)|^2 \tag{13}$$

This error is to be minimized over the entire volume for which the numerical results exist. Thus,

$$J'(\tilde{\alpha}_{ij},\tilde{\beta}_{ij}) = \int_0^{2\pi}\int_0^{\pi}\int_{r_{min}}^{r_{max}} J(r,\phi,\lambda) r^2\sin(\phi) dr d\phi d\lambda \tag{14}$$

This is now an unconstrained minimization problem where $J'(\tilde{\alpha}_{ij},\tilde{\beta}_{ij})$ is to be minimized using $\tilde{\alpha}_{ij}$ and $\tilde{\beta}_{ij}$ as the variables. The minimization problem can be formulated as

$$\min_{\tilde{\alpha}_{ij},\tilde{\beta}_{ij}} J'(\tilde{\alpha}_{ij},\tilde{\beta}_{ij})$$

where

$$\begin{aligned}\frac{\partial J'(\tilde{\alpha}_{ij},\tilde{\beta}_{ij})}{\partial\tilde{\alpha}_{ij}} &= \int_{r_{min}}^{r_{max}}\int_0^{\pi}\int_0^{2\pi} r^2(\mathcal{P}_n - \mathcal{P}_a)\left(-\frac{\partial\mathcal{P}_a}{\partial\tilde{\alpha}_{ij}}\right) r^2\sin(\phi) dr d\phi d\lambda \\ &= -\int_{r_{min}}^{r_{max}}\int_0^{\pi}\int_0^{2\pi} (\mathcal{P}_n - \mathcal{P}_a) P(\cos\phi)\cos(j\lambda) r^2\sin(\phi) dr d\phi d\lambda \end{aligned} \tag{15}$$

and

$$\begin{aligned}\frac{\partial J'(\tilde{\alpha}_{ij},\tilde{\beta}_{ij})}{\partial\tilde{\beta}_{ij}} &= \int_{r_{min}}^{r_{max}}\int_0^{\pi}\int_0^{2\pi} r^2(\mathcal{P}_n - \mathcal{P}_a)\left(-\frac{\partial\mathcal{P}_a}{\partial\tilde{\beta}_{ij}}\right) r^2\sin(\phi) dr d\phi d\lambda \\ &= -\int_{r_{min}}^{r_{max}}\int_0^{\pi}\int_0^{2\pi} (\mathcal{P}_n - \mathcal{P}_a) P(\cos\phi)\sin(j\lambda) r^2\sin(\phi) dr d\phi d\lambda \end{aligned} \tag{16}$$

Setting $[\partial J'(\tilde{\alpha}_{ij},\tilde{\beta}_{ij})]/\partial\tilde{\alpha}_{ij} = 0$ and $[\partial J'(\tilde{\alpha}_{ij},\tilde{\beta}_{ij})]/\partial\tilde{\beta}_{ij} = 0$ to minimize $J'(\tilde{\alpha}_{ij},\tilde{\beta}_{ij})$ yields

$$\int_{r_{min}}^{r_{max}} \int_0^{\pi} \int_0^{2\pi} \mathcal{P}_n P_{ij}(\cos\phi)\cos(j\lambda) r^2 \sin(\phi) dr d\phi d\lambda =$$

$$\int_{r_{min}}^{r_{max}} \int_0^{\pi} \int_0^{2\pi} \mathcal{P}_a P(\cos\phi)\cos(j\lambda) r^2 \sin(\phi) dr d\phi d\lambda \tag{17}$$

and

$$\int_{r_{min}}^{r_{max}} \int_0^{\pi} \int_0^{2\pi} \mathcal{P}_n P_{ij}(\cos\phi)\sin(j\lambda) r^2 \sin(\phi) dr d\phi d\lambda =$$

$$\int_{r_{min}}^{r_{max}} \int_0^{\pi} \int_0^{2\pi} \mathcal{P}_a P(\cos\phi)\sin(j\lambda) r^2 \sin(\phi) dr d\phi d\lambda \tag{18}$$

The integral on the left-hand side of these equations can be approximated by a summation over the entire volume of interest using small values of Δr, $\Delta\phi$, and $\Delta\lambda$. Substituting for $\mathcal{P}_a$ in the right-hand side and using the properties of the associated Legendre polynomials given in Eqs. (6) through (9) yields

$$\sum_{k=r_{min}}^{r_{max}} \sum_{l=0}^{\pi} \sum_{m=0}^{2\pi} \mathcal{P}_n P_{ij}(\cos\phi_l)\cos(j\lambda_m) r_k^2 \sin(\phi_l) \Delta r \Delta\phi \Delta\lambda$$

$$= \int_{r_{min}}^{r_{max}} \int_0^{\pi} \int_0^{2\pi} \left(\frac{1}{r^2} \sum_{k=0}^{N} \sum_{l=0}^{k} P_{kl}(\cos\phi) \left[\tilde{\alpha}_{kl}\cos(l\lambda) + \tilde{\beta}_{kl}\sin(l\lambda) \right] \right)$$

$$\times P_{ij}(\cos\phi)\cos(j\lambda) r^2 \sin(\phi) dr d\phi d\lambda$$

$$= \sum_{k=0}^{N} \sum_{l=0}^{k} \int_{r_{min}}^{r_{max}} \int_0^{2\pi} \left(\int_0^{\pi} P_{kl} P_{ij} \sin(\phi) d\phi \right)$$

$$\times \left[\tilde{\alpha}_{kl}\cos(l\lambda)\cos(j\lambda) + \tilde{\beta}_{kl}\sin(l\lambda)\cos(j\lambda) \right] dr d\lambda$$

$$= \frac{(i+j)!}{(i-j)!} \frac{2}{2i+1} \int_{r_{min}}^{r_{max}} \int_0^{2\pi} \left[\tilde{\alpha}_{ij}\cos^2(j\lambda) + \tilde{\beta}_{ij}\sin(j\lambda)\cos(j\lambda) \right] dr d\lambda$$

$$= [r_{max} - r_{min}] \frac{(i+j)!}{(i-j)!} \frac{2}{2i+1} \tilde{\alpha}_{ij} \int_0^{2\pi} \cos^2(j\lambda) d\lambda$$

$$= [r_{max} - r_{min}] \frac{2}{2i+1} \tilde{\alpha}_{i0} [2\pi] \quad \text{for } j = 0$$

$$= [r_{max} - r_{min}] \frac{(i+j)!}{(i-j)!} \frac{2}{2i+1} \tilde{\alpha}_{ij} [\pi] \quad \text{for } j > 0 \tag{19}$$

Similarly,

$$\sum_{k=r_{min}}^{r_{max}} \sum_{l=0}^{\pi} \sum_{m=0}^{2\pi} \mathcal{P}_n P_{ij}(\cos\phi_l)\sin(j\lambda_m) r_k^2 \sin(\phi_l)\Delta r \Delta\phi\Delta\lambda$$

$$= \int_{r_{min}}^{r_{max}} \int_0^{\pi} \int_0^{2\pi} \left(\frac{1}{r^2} \sum_{k=0}^{N} \sum_{l=0}^{k} P_{kl}(\cos\phi) \left[\tilde{\alpha}_{kl}\cos(l\lambda) + \tilde{\beta}_{kl}\sin(l\lambda) \right] \right)$$

$$\times P_{ij}(\cos\phi)\sin(j\lambda) r^2 \sin(\phi) dr d\phi d\lambda$$

$$= \sum_{k=0}^{N} \sum_{l=0}^{k} \int_{r_{min}}^{r_{max}} \int_0^{2\pi} \left(\int_0^{\pi} P_{kl} P_{ij} \sin(\phi) d\phi \right)$$

$$\times \left[\tilde{\alpha}_{kl}\cos(l\lambda)\sin(j\lambda) + \tilde{\beta}_{kl}\sin(l\lambda)\sin(j\lambda) \right] dr d\lambda$$

$$= \frac{(i+j)!}{(i-j)!} \frac{2}{2i+1} \int_{r_{min}}^{r_{max}} \int_0^{2\pi} \left[\tilde{\alpha}_{ij}\cos(j\lambda)\sin(j\lambda) + \tilde{\beta}_{ij}\sin^2(j\lambda) \right] dr d\lambda$$

$$= [r_{max} - r_{min}] \frac{(i+j)!}{(i-j)!} \frac{2}{2i+1} \tilde{\beta}_{ij} \int_0^{2\pi} \sin^2(j\lambda) d\lambda$$

$$= [r_{max} - r_{min}] \frac{(i+j)!}{(i-j)!} \frac{2}{2i+1} \tilde{\beta}_{ij} [\pi] \quad \text{for } j > 0 \tag{20}$$

The parameters $\tilde{\alpha}_{ij}$ and $\tilde{\beta}_{ij}$ then are solved from the equations and are used to determine the parameters $\mathcal{P}_d$, α_{ij}, and β_{ij}.

IV. Numerical Results

The mathematical model proposed in the previous section was tested using the numerical simulation data created for comet Tempel-1 and comet Wirtanen for a number of distances from the Sun [1].

A. Tempel-1 Results

The comet Tempel-1 was modeled as a spherical nucleus of radius 3 km. Outgassing pressure fields were generated for comet–Sun distances of 1.5, 2.0, 2.8, and 3.4 AU. The nucleus rotation is not taken into account in this simulation. The pressure field was computed over a radius range of from 10 to 25 km from the comet.

Since the equations to solve for the coefficients $\tilde{\alpha}'_{ij}s$ and $\tilde{\beta}'_{ij}s$ are uncoupled, they are solved as simple algebraic equations. The coefficient values for each case are given in the Appendix. These coefficients were then substituted into Eq. (1) to generate the analytical field.

The analytically generated drag field and the numerically simulated drag field at a radial distance of 19.5 km, and when the comet nucleus is at a distance of 2.0 AU from the Sun, are shown in Figs. 2 and 3,

respectively. The fractional and absolute error contours between the two are shown in Figs. 4 and 5, respectively. Figures 6 through 8 show the fractional error plots, at the same radial distance of 19.5 km, when the nucleus is at 1.5, 2.8, and 3.4 AU from the Sun, respectively.

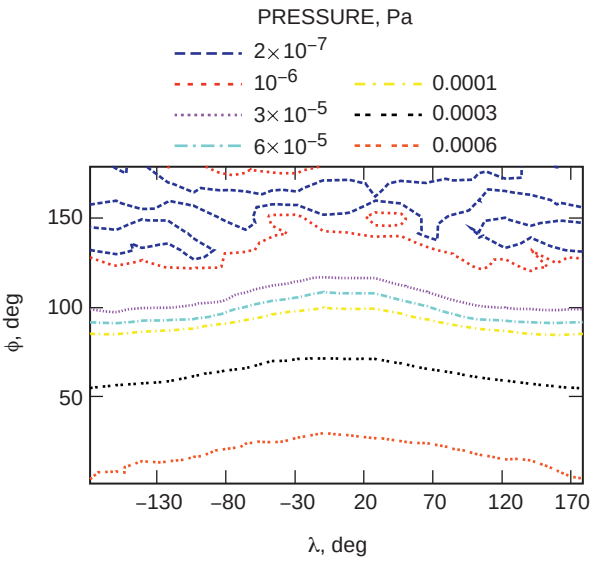

Fig. 2. Tempel-1 drag field generated analytically (2.0 AU at 19.5 km).

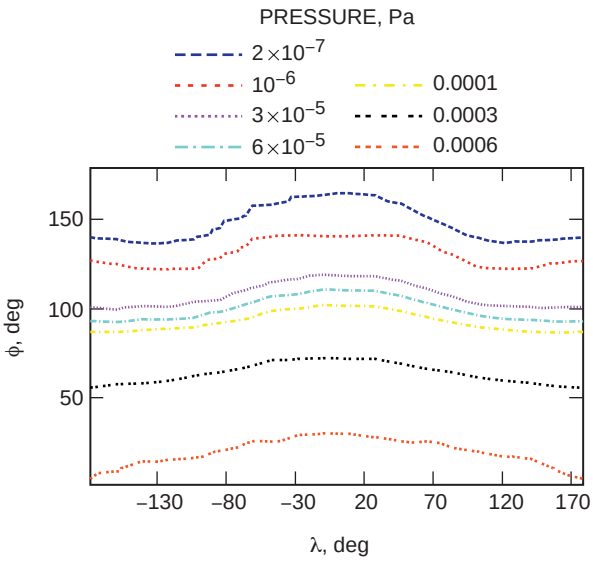

Fig. 3. Tempel-1 drag field simulated numerically (2.0 AU at 19.5 km).

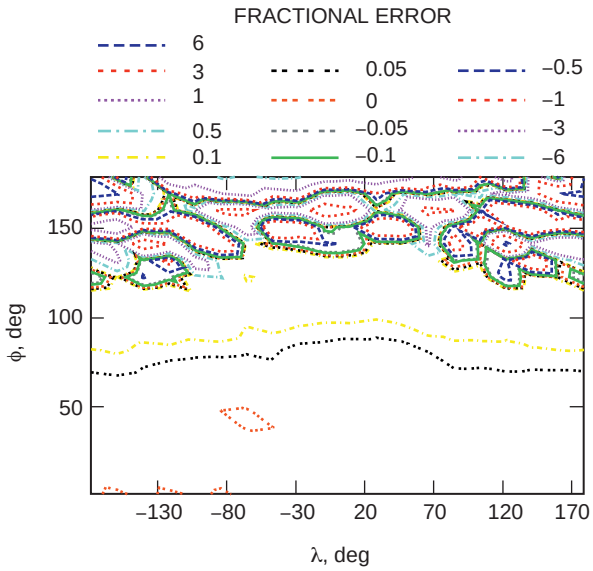

Fig. 4. Tempel-1 drag field fractional error contours (2.0 AU at 19.5 km).

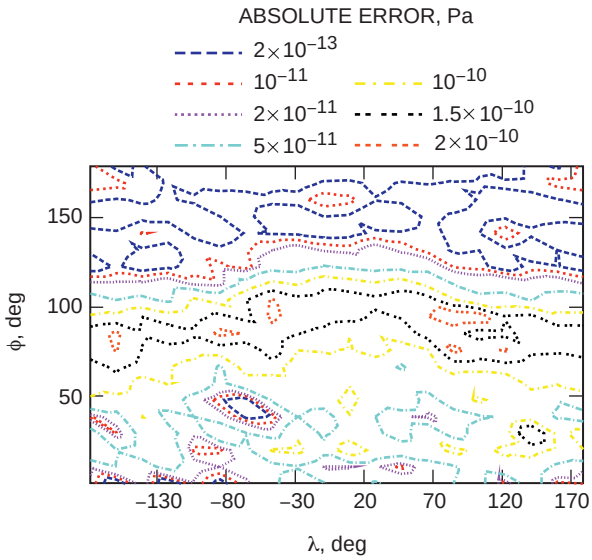

Fig. 5. Tempel-1 drag field absolute error contours (2.0 AU at 19.5 km).

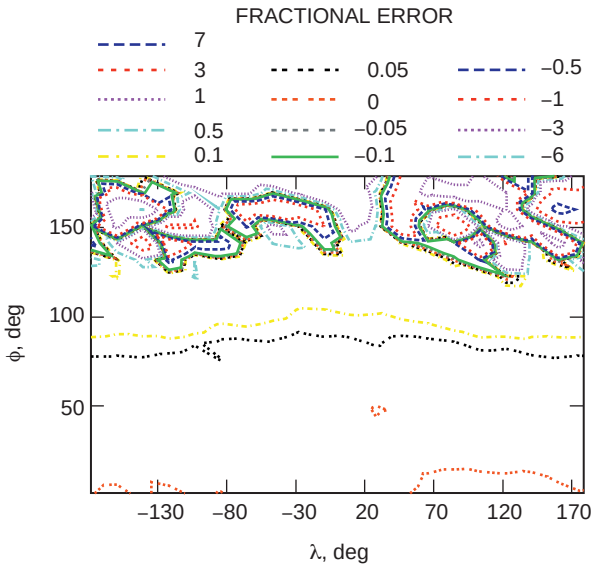

Fig. 6. Tempel-1 drag field fractional error contours (1.5 AU at 19.5 km).

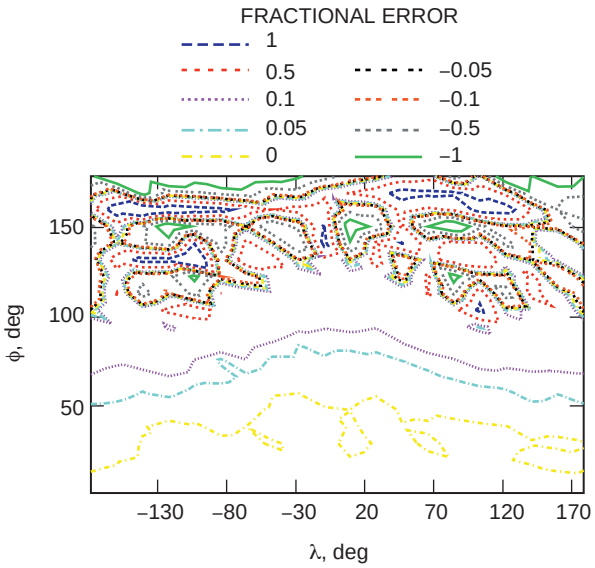

Fig. 7. Tempel-1 drag field fractional error contours (2.8 AU at 19.5 km).

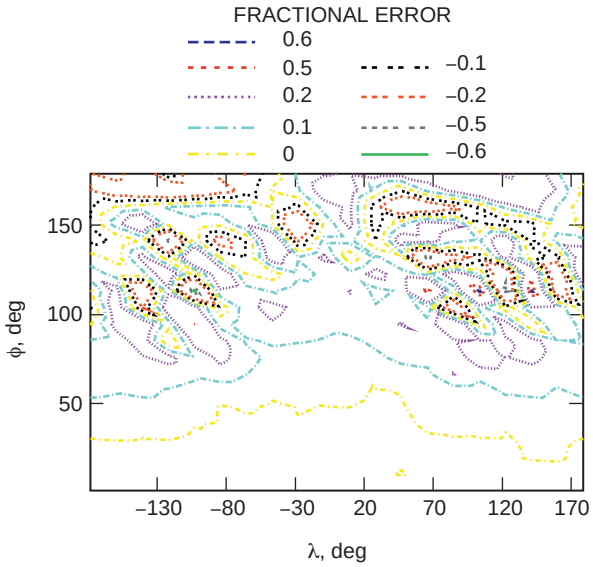

Fig. 8. Tempel-1 drag field fractional error contours (3.4 AU at 19.5 km).

The fractional error is computed as

$$\text{fractional error} = \frac{\mathcal{P}_n - \mathcal{P}_a}{\mathcal{P}_n}$$

The absolute error is calculated as

$$\text{absolute error} = \frac{\mathcal{P}_n - \mathcal{P}_a}{\mathcal{P}_d}$$

B. Wirtanen Results

The comet Wirtanen is modeled as a sphere of radius 600.0 m. The nucleus rotates with a period of 10 hours, and its spin axis is perpendicular to the comet's orbital plane. Data have been generated for Sun–comet distances of 1, 2, 3, and 4 AU.

The pressure field was computed over a range of radii from 1 to 10 km. All the results presented are for the drag distribution at a radial distance of 5.2 km from the nucleus of the comet.

The numerically simulated drag field when the comet is at a distance of 1 AU from the Sun is shown in Fig. 9. The fractional error contours in the phi–lambda plane are shown in Fig. 10. Fractional error plots for the other cases are shown in Figs. 11 through 13. The fit parameter values are given in the Appendix.

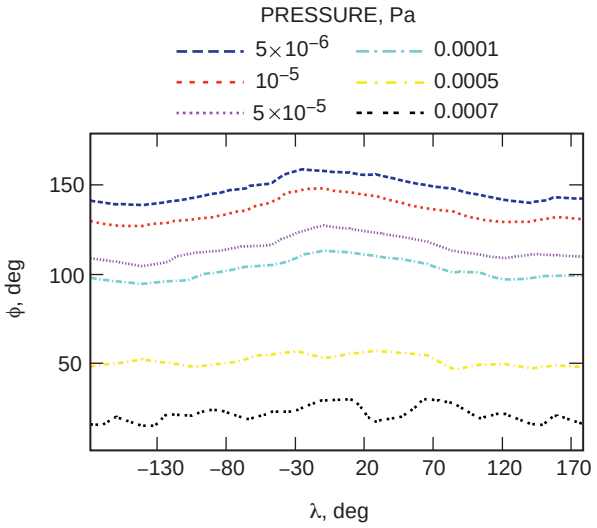

Fig. 9. Wirtanen drag field simulated numerically (1.0 AU at 5200.0 m).

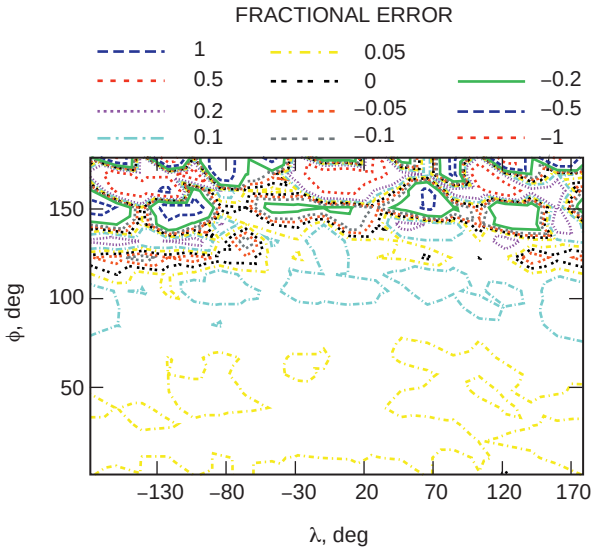

Fig. 10. Wirtanen fractional error contours (1.0 AU at 5200.0 m).

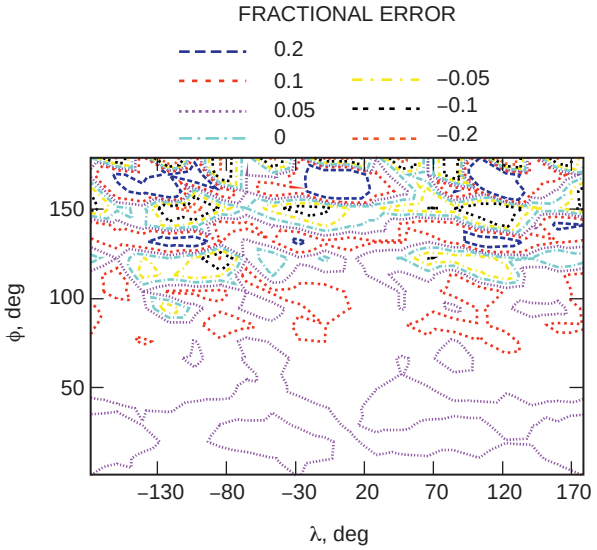

Fig. 11. Wirtanen fractional error contours (2.0 AU at 5200.0 m).

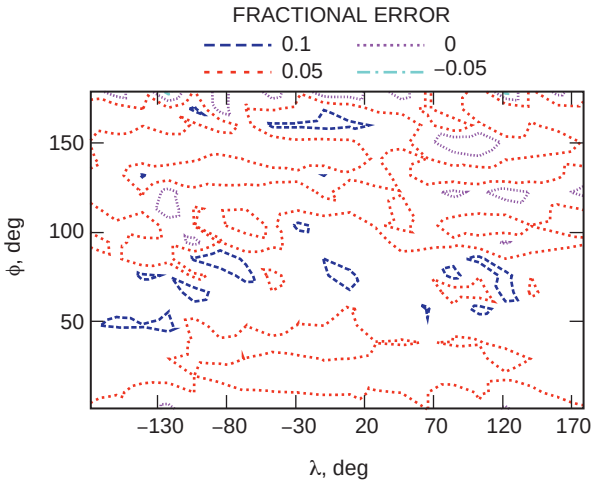

Fig. 12. Wirtanen fractional error contours (3.0 AU at 5200.0 m).

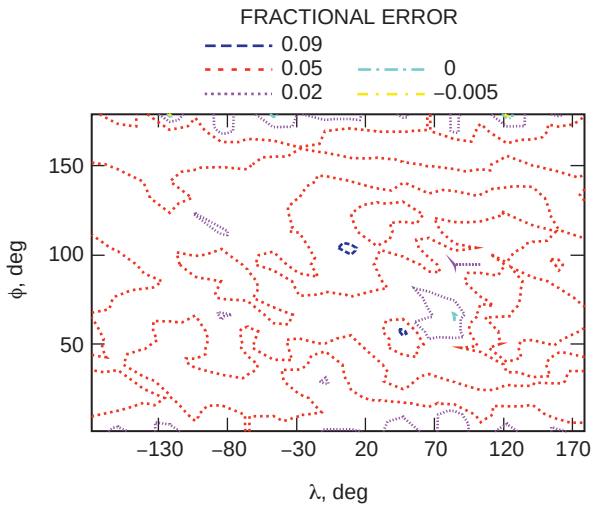

Fig. 13. Wirtanen fractional error contours (4.0 AU at 5200.0 m).

V. Conclusion

A mathematical model to simulate the comet force environment has been developed and described. The model was tested using numerical simulations for comets Tempel-1 and Wirtanen for different distances from the Sun. Parameter coefficients for the model were obtained using the method of least squares. The results were represented as contour plots showing the fractional error between the drag pressure values obtained from numerical simulations and those from the analytical expression.

The results of the study show that the drag is modeled well by the mathematical formulation. The largest relative errors were found in the antisolar region where the magnitude of drag pressure is very small, and, hence, the absolute errors are small as well. Otherwise, the errors are within 10 to 15 percent. Given that we are modeling a complex gas dynamical problem with a relatively simple analytical model, this level of agreement appears promising.

These analytical drag pressure values can be used to compute the acceleration produced on a spacecraft in the vicinity of a comet. Given a parameterization of the pressure field, it becomes possible to estimate the values of the coefficients by tracking the motion of the spacecraft with radio metric data.

References

[1] A. Enzian, P. R. Weissman, R. W. Gaskell, D. G. Goodwin, D. J. Scheeres, and S. Bhargava, "Periodic Comets 46P/Wirtanen and 9P/Tempel 1: Gas Dynamical Modeling of the Near-Nucleus Coma Environment," Poster 14.17-P, presented at the Asteroids, Comet, Meteors 2000 Meeting, Cornell University, Ithaca, New York, July 2000.

[2] J. K. Miller, C. J. Weeks, and L. J. Wood, "Orbit Determination Strategy and Accuracy for a Comet Rendezvous Mission," *Journal of Guidance, Control, and Dynamics*, vol. 13, no. 5, pp. 775–784, 1990.

[3] M. A. Pinsky, *Introduction to Partial Differential Equations with Application*, New York: McGraw-Hill Book Company, 1984.

[4] D. J. Scheeres, F. Marzari, L. Tomasella, and V. Vanzani, "ROSETTA Mission: Satellite Orbits Around a Cometary Nucleus," *Planetary and Space Science*, vol. 46, no. 6/7, pp. 649–671, 1998.

[5] C. J. Weeks, "The Effect of Comet Outgassing and Dust Emission on the Navigation of an Orbiting Spacecraft," Paper AAS 93-624, in *Advances in the Astronautical Sciences, Astrodynamics 1993*, vol. 85, Univelt, pp. 1313–1330.

Appendix

Comet Outgassing Model Parameters

The $\mathcal{P}_d$, $\alpha_{i,j}$, and $\beta_{i,j}$ parameters used in the mathematical model are found by performing a least-squares fit between the data and the model. The coefficients are calculated up to the fourth degree and order for comets Tempel-1 and Wirtanen at different distances from the Sun and are presented in Tables A-1 through A-10.

I. Parameter Values for Tempel-1

The value of $\mathcal{P}_d$, which is a measure of the overall strength of the drag pressure field, is shown in Table A-1.

II. Parameter Values for Wirtanen

The value of $\mathcal{P}_d$, which is a measure of the overall strength of the drag pressure field, is shown in Table A-6.

Table A-1. $\mathcal{P}_d$ values for comet Tempel-1.

Distance from the Sun, AU	$\mathcal{P}_d$, Pa-km^2
1.5	1.80934×10^{-1}
2.0	6.960×10^{-2}
2.8	1.299×10^{-2}
3.4	1.978×10^{-3}

Table A-2. Coefficients for comet Tempel-1 (at 1.5 AU from the Sun).

i	j	α_{ij}	β_{ij}
0	0	1.0000000×10^{0}	0.0000000×10^{0}
1	0	1.6513830×10^{0}	0.0000000×10^{0}
1	1	2.0728170×10^{-1}	2.5017790×10^{-4}
2	0	6.4367780×10^{-1}	0.0000000×10^{0}
2	1	7.8335950×10^{-2}	$-5.9572510 \times 10^{-4}$
2	2	8.8972100×10^{-3}	$-3.6459290 \times 10^{-4}$
3	0	$-6.5870240 \times 10^{-2}$	0.0000000×10^{0}
3	1	$-6.9419650 \times 10^{-3}$	$-1.5515240 \times 10^{-3}$
3	2	$-2.3754830 \times 10^{-3}$	$-6.3998910 \times 10^{-4}$
3	3	$-5.0360360 \times 10^{-4}$	1.6641230×10^{-4}
4	0	$-3.3786880 \times 10^{-2}$	0.0000000×10^{0}
4	1	$-1.2865270 \times 10^{-3}$	$-1.4554300 \times 10^{-3}$
4	2	$-1.9933410 \times 10^{-3}$	$-2.3050640 \times 10^{-4}$
4	3	$-1.6764510 \times 10^{-4}$	5.2290180×10^{-5}
4	4	$-4.9717790 \times 10^{-5}$	$-2.7762220 \times 10^{-5}$

Table A-3. Coefficients for comet Tempel-1 (at 2.0 AU from the Sun).

i	j	α_{ij}	β_{ij}
0	0	1.0000000×10^{0}	0.0000000×10^{0}
1	0	1.7424380×10^{0}	0.0000000×10^{0}
1	1	2.4954340×10^{-1}	$-3.2874030 \times 10^{-3}$
2	0	8.0649220×10^{-1}	0.0000000×10^{0}
2	1	1.0767340×10^{-1}	$-1.7287340 \times 10^{-3}$
2	2	1.2179830×10^{-2}	4.2847190×10^{-4}
3	0	$-1.6492650 \times 10^{-2}$	0.0000000×10^{0}
3	1	$-4.0825580 \times 10^{-3}$	3.1134650×10^{-3}
3	2	$-1.5942440 \times 10^{-3}$	$-7.3604510 \times 10^{-4}$
3	3	$-3.3663670 \times 10^{-4}$	$-1.3549240 \times 10^{-4}$
4	0	$-6.4582310 \times 10^{-2}$	0.0000000×10^{0}
4	1	$-9.6370230 \times 10^{-4}$	4.2770650×10^{-3}
4	2	$-2.0065580 \times 10^{-3}$	$-5.6703060 \times 10^{-4}$
4	3	$-9.4770940 \times 10^{-5}$	$-9.6860660 \times 10^{-5}$
4	4	$-1.2518440 \times 10^{-4}$	2.1226330×10^{-5}

Table A-4. Coefficients for comet Tempel-1 (at 2.8 AU from the Sun).

i	j	α_{ij}	β_{ij}
0	0	1.0000000×10^{0}	0.0000000×10^{0}
1	0	1.8997880×10^{0}	0.0000000×10^{0}
1	1	3.8985930×10^{-1}	9.8821320×10^{-4}
2	0	1.1413790×10^{0}	0.0000000×10^{0}
2	1	2.2495110×10^{-1}	2.9750430×10^{-3}
2	2	3.0701350×10^{-2}	$-4.7119580 \times 10^{-3}$
3	0	1.6240230×10^{-1}	0.0000000×10^{0}
3	1	2.4372550×10^{-2}	5.6541470×10^{-3}
3	2	4.8925980×10^{-3}	$-3.9677030 \times 10^{-3}$
3	3	$-6.3294680 \times 10^{-5}$	2.8249220×10^{-4}
4	0	$-1.0326560 \times 10^{-1}$	0.0000000×10^{0}
4	1	$-1.9340210 \times 10^{-2}$	6.8011610×10^{-3}
4	2	$-3.0078680 \times 10^{-3}$	$-1.6124520 \times 10^{-3}$
4	3	$-9.7242890 \times 10^{-5}$	2.7675040×10^{-5}
4	4	$-7.1400310 \times 10^{-5}$	$-3.9291900 \times 10^{-5}$

Table A-5. Coefficients for comet Tempel-1 (at 3.4 AU from the Sun).

i	j	α_{ij}	β_{ij}
0	0	1.0000000×10^{0}	0.0000000×10^{0}
1	0	1.9800110×10^{0}	0.0000000×10^{0}
1	1	5.4047670×10^{-1}	1.4208230×10^{-3}
2	0	1.3961880×10^{0}	0.0000000×10^{0}
2	1	3.7278940×10^{-1}	6.8037350×10^{-3}
2	2	5.3518230×10^{-2}	$-4.5266220 \times 10^{-3}$
3	0	3.7225700×10^{-1}	0.0000000×10^{0}
3	1	8.7147080×10^{-2}	8.8218460×10^{-3}
3	2	1.4803090×10^{-2}	$-8.8016460 \times 10^{-4}$
3	3	1.9673480×10^{-3}	$-8.6774620 \times 10^{-4}$
4	0	$-9.7046410 \times 10^{-2}$	0.0000000×10^{0}
4	1	$-3.3845070 \times 10^{-2}$	6.4254570×10^{-3}
4	2	$-4.5740620 \times 10^{-3}$	8.4873090×10^{-4}
4	3	1.2154710×10^{-5}	$-3.3200540 \times 10^{-4}$
4	4	$-8.8424940 \times 10^{-5}$	1.2160880×10^{-5}

Table A-6. $\mathcal{P}_d$ values for comet Wirtanen.

Distance from the Sun, AU	$\mathcal{P}_d$, Pa-km^2
1.5	6.29091×10^{-3}
2.0	1.08287×10^{-3}
2.8	1.7687×10^{-4}
3.4	6.681×10^{-5}

Table A-7. Coefficients for comet Wirtanen (at 1.0 AU from the Sun).

i	j	α_{ij}	β_{ij}
0	0	1.0000000×10^{0}	0.0000000×10^{0}
1	0	1.5439460×10^{0}	0.0000000×10^{0}
1	1	1.4926630×10^{-1}	9.8506420×10^{-3}
2	0	5.5570930×10^{-1}	0.0000000×10^{0}
2	1	2.7821960×10^{-2}	$-3.3019840 \times 10^{-3}$
2	2	8.1902740×10^{-3}	7.4885970×10^{-4}
3	0	$-2.8099460 \times 10^{-2}$	0.0000000×10^{0}
3	1	$-1.3797980 \times 10^{-2}$	$-4.5269840 \times 10^{-3}$
3	2	$-3.3052540 \times 10^{-3}$	4.0772180×10^{-4}
3	3	$-2.3958030 \times 10^{-4}$	9.0932100×10^{-4}
4	0	$-3.0644360 \times 10^{-2}$	0.0000000×10^{0}
4	1	4.2688560×10^{-3}	2.9656240×10^{-3}
4	2	$-7.9570710 \times 10^{-4}$	3.8809930×10^{-4}
4	3	$-1.7614530 \times 10^{-4}$	$-4.9953990 \times 10^{-5}$
4	4	4.0438070×10^{-5}	$-1.1341220 \times 10^{-4}$

Table A-8. Coefficients for comet Wirtanen (at 2.0 AU from the Sun).

i	j	α_{ij}	β_{ij}
0	0	1.0000000×10^{0}	0.0000000×10^{0}
1	0	1.6267360×10^{0}	0.0000000×10^{0}
1	1	2.2982820×10^{-1}	1.8094370×10^{-3}
2	0	8.0524860×10^{-1}	0.0000000×10^{0}
2	1	9.1647530×10^{-2}	$-3.9811900 \times 10^{-3}$
2	2	1.4224620×10^{-2}	$-7.5582360 \times 10^{-4}$
3	0	6.6195180×10^{-2}	0.0000000×10^{0}
3	1	$-9.6985340 \times 10^{-3}$	$-7.4465090 \times 10^{-3}$
3	2	3.5376810×10^{-4}	$-1.8622190 \times 10^{-3}$
3	3	4.8860450×10^{-4}	4.3628770×10^{-4}
4	0	$-5.0343020 \times 10^{-2}$	0.0000000×10^{0}
4	1	$-1.3256430 \times 10^{-2}$	$-7.1021330 \times 10^{-3}$
4	2	1.0357320×10^{-4}	$-6.0426040 \times 10^{-4}$
4	3	$-2.6067180 \times 10^{-4}$	$-3.1910070 \times 10^{-5}$
4	4	8.1056070×10^{-5}	$-1.2931220 \times 10^{-5}$

Table A-9. Coefficients for comet Wirtanen (at 3.0 AU from the Sun).

i	j	α_{ij}	β_{ij}
0	0	1.0000000×10^{0}	0.0000000×10^{0}
1	0	1.2331050×10^{0}	0.0000000×10^{0}
1	1	2.9131200×10^{-1}	$-4.6131910 \times 10^{-3}$
2	0	8.3801860×10^{-1}	0.0000000×10^{0}
2	1	1.8806740×10^{-1}	$-1.4711880 \times 10^{-2}$
2	2	2.6529030×10^{-2}	$-6.2771310 \times 10^{-3}$
3	0	2.0129810×10^{-1}	0.0000000×10^{0}
3	1	4.3985800×10^{-2}	$-1.8254850 \times 10^{-2}$
3	2	2.1298700×10^{-3}	$-2.5285840 \times 10^{-3}$
3	3	6.0355120×10^{-4}	$-5.7993490 \times 10^{-4}$
4	0	$-6.8328580 \times 10^{-2}$	0.0000000×10^{0}
4	1	$-1.0229320 \times 10^{-2}$	$-1.5446970 \times 10^{-2}$
4	2	$-4.1219380 \times 10^{-3}$	$-1.5067660 \times 10^{-5}$
4	3	$-3.6627740 \times 10^{-4}$	$-3.9370520 \times 10^{-4}$
4	4	6.2601620×10^{-5}	1.4355990×10^{-4}

Table A-10. Coefficients for comet Wirtanen (at 4.0 AU from the Sun).

i	j	α_{ij}	β_{ij}
0	0	1.0000000×10^{0}	0.0000000×10^{0}
1	0	8.4294760×10^{-2}	0.0000000×10^{0}
1	1	3.6461650×10^{-2}	1.2179120×10^{-2}
2	0	8.1575390×10^{-2}	0.0000000×10^{0}
2	1	$-1.9576060 \times 10^{-3}$	2.4195540×10^{-3}
2	2	8.6259410×10^{-3}	1.5244460×10^{-3}
3	0	$-1.2969440 \times 10^{-2}$	0.0000000×10^{0}
3	1	$-2.3357440 \times 10^{-3}$	$-6.6894900 \times 10^{-4}$
3	2	$-6.8463370 \times 10^{-4}$	1.9253250×10^{-3}
3	3	5.1682880×10^{-4}	3.8230850×10^{-4}
4	0	$-5.2120180 \times 10^{-3}$	0.0000000×10^{0}
4	1	$-1.6789200 \times 10^{-3}$	$-2.6434480 \times 10^{-4}$
4	2	1.8813310×10^{-3}	$-2.0996490 \times 10^{-4}$
4	3	$-5.9608600 \times 10^{-5}$	2.2950560×10^{-4}
4	4	1.0498750×10^{-4}	1.7102570×10^{-5}